Transient and asymptotic behaviour of the binary breakage problem

2005 J. Phys. A: Math. Gen. 38 5111

(http://iopscience.iop.org/0305-4470/38/23/004)

INSTITUTE OF PHYSICS PUBLISHING JOURNAL OF PHYSICS A: MATHEMATICAL AND GENERAL

J. Phys. A: Math. Gen. **38** (2005) 5111–5132 doi:10.1088/0305-4470/38/23/004

Transient and asymptotic behaviour of the binary breakage problem

Nikos V Mantzaris

Department of Chemical and Biomolecular Engineering and Bioengineering Department, Rice University, Houston, TX 77005, USA

E-mail: nman@rice.edu

Received 17 January 2005, in final form 4 April 2005
Published 25 May 2005
Online at stacks.iop.org/JPhysA/38/5111

Abstract

The general binary breakage problem with power-law breakage functions and two families of symmetric and asymmetric breakage kernels is studied in this work. A useful transformation leads to an equation that predicts self-similar solutions in its asymptotic limit and offers explicit knowledge of the mean size and particle density at each point in dimensionless time. A novel moving boundary algorithm in the transformed coordinate system is developed, allowing the accurate prediction of the full transient behaviour of the system from the initial condition up to the point where self-similarity is achieved, and beyond if necessary. The numerical algorithm is very rapid and its results are in excellent agreement with known analytical solutions. In the case of the symmetric breakage kernels only unimodal, self-similar number density functions are obtained asymptotically for all parameter values and independent of the initial conditions, while in the case of asymmetric breakage kernels, bimodality appears for high degrees of asymmetry and sharp breakage functions. For symmetric and discrete breakage kernels, self-similarity is not achieved. The solution exhibits sustained oscillations with amplitude that depends on the initial condition and the sharpness of the breakage mechanism, while the period is always fixed and equal to ln 2 with respect to dimensionless time.

PACS numbers: 02.60.Nm, 68.43.Jk, 82.30.Lp

(Some figures in this article are in colour only in the electronic version)

1. Introduction

Breakage is the process by which an initial particle population breaks to give more particles of smaller size. It is known in the literature by many names such as fragmentation or milling or

scission or partition or disintegration or division as well as others. Breakage is encountered in a wide variety of physical phenomena and engineering applications, such as polymer degradation [1], coal combustion [2], grinding [3], crystallization [4], break-up of liquid droplets or air bubbles [5], as well as cell division of cells in a population [6]. Redner *et al* [7] offer an extensive listing of processes in science and engineering where breakage plays a fundamental role.

A pure, linear breakage process is mathematically described by a partial integro-differential equation, known as a population balance equation [8]. It is fully characterized by two functions. First, the breakage rate or breakage function, which describes the rate by which a particle of size x breaks to give smaller particles, and second, the breakage kernel (also known as partition probability density function in the context of cell population dynamics) which describes the probability that a mother particle will partition, upon breakage, into daughter particles of smaller sizes. In the case where each breakage event leads to the production of two daughter particles, the process is called binary breakage, while in the case where more daughter particles are produced, the process is known as multiple break-up.

While the most frequently used breakage function is of the power law type, there are several different classes of breakage kernels. For binary breakage processes (which will be the focus of this work), if the highest probability is to produce two equally sized daughter particles from each breakage event, then the breakage kernel is called symmetric, whereas if this is not the case, it is called asymmetric. Moreover, when the binary breakage kernel can be expressed as a function of the daughter to mother particle size ratio divided by the mother particle size, the breakage kernel is called homogeneous. Furthermore, when the breakage kernel is independent of the size of the daughter particle, the process is called uniform breakage or random scission. Another important classification of breakage kernels is in continuous and discrete. In the former case, the breakage kernel is a continuous function, thus allowing more than one outcome of each breakage event. If the highest probability is for an equal split, then the breakage kernel is continuous and symmetric, otherwise it is continuous and asymmetric. In the case of a discrete breakage kernel, each breakage event always has the exact same outcome. For example, in the case of asymmetric and discrete breakage, each breakage event leads to the production of a daughter particle with a fraction r of the mother particle content and a daughter particle with a fraction $(1 - r)$ of the mother particle content. This type of breakage kernel is mathematically expressed as a sum of delta functions, thus allowing only one possibility for the sizes of the daughter particles born from a mother particle of a given size. In this work, in an effort to be as general as possible, we will consider a whole family of homogeneous, symmetric breakage kernels and a family of discrete, asymmetric breakage kernels.

An exceptional body of work has been devoted to the analytical treatment of the problem. We note the excellent work of Ziff and McGrady [9, 10] and Ziff [11] who derived full transient solutions for several cases of power-law breakage functions and for specific breakage kernels. Kostoglou *et al* [12] and Kostoglou and Karabelas [13] developed solutions of the steady-state breakage equation with homogeneous breakage kernels in the case of a maximum stable size. Furthermore, Ziff and McGrady [1] applied the method of successive generations to derive analytical approximations for special types of binary breakage processes, while Kostoglou and Karabelas [14] generalized this approach for multiple break-up and for a special type of asymmetric homogeneous breakage kernel known as the erosion kernel.

A fundamental characteristic of breakage processes is the existence of asymptotic self-similar behaviour in which the solution behaves as a function of one variable resulting from a special grouping of the two independent variables of size and time. Filippov [15] was the first to show the existence of such solutions by formulating the problem as a one-dimensional Markov

process. Cheng and Redner [16] used elegant arguments and the scaling *ansatz* first presented by Friedlander and Wang [17] to prove that the self-similar solution is unique for positive powers of power-law breakage functions and homogeneous breakage kernels. Moreover, Treat [18] constructed self-similar solutions for the same type of breakage functions and polynomial expressions for the breakage kernel. Madras and McCoy [19] expressed the size distribution using generalized gamma distribution parameters and analytically described the evolution of these parameters towards self-similarity in the cases of linear breakage functions and a discrete symmetric breakage kernel, as well as in the case where the breakage kernel is independent of the size of the daughter particles. Recently, Kostoglou [20] presented self-similar solutions in the case of discrete asymmetric breakage kernels.

Despite the invaluable insights that can be obtained from such analytical approaches, the generality of the problem is best served by numerical efforts. To this end, Hill and Ng [21] discretized the binary breakage equation using either an equidistant or a geometric grid. They considered power-law breakage functions and three different breakage kernels: (a) uniform (independent of daughter particle size), (b) parabolic and (c) empirical. For each type, they derived special coefficients that were specific to the type of grid used as well as to the type of breakage kernel, by matching the zeroth and first moments of the discretized equations with those of the continuous population balance equation. The same investigators later extended their approach to multiple breakage processes [22]. Despite the success in simulating various breakage processes this approach requires the derivation of specific coefficients for each type of breakage kernel. Vanni [23] addressed this problem by modifying their algorithm appropriately to demand exact agreement with the population balance equation in the approximation of the breakage term instead of the particle density. However, the price of this generalization was that his results were slightly worse than those of Hill and Ng for two breakage kernels, in terms of the first four moments of the distribution. Moreover, Liu and Tade [24] recently developed an adaptive wavelet-based method to solve the uniform binary breakage problem and the problem of multiple break-up. Their results were found to be in agreement with analytical solutions for two different points in time and two breakage kernels.

The aforementioned numerical efforts all share one common characteristic: they discretize the original breakage equation directly. In pure breakage processes the particle density tends to infinity, while the mean size tends to zero. Due to the particular physics of the problem, any numerical method discretizing directly the original breakage equation is bound to run into inaccuracies of some kind for large times, as was indeed observed in some of these efforts [21]. In addition, such approaches do not naturally reveal the self-similar nature of breakage equations that was so elegantly shown in several analytical efforts. As a result of these characteristics, full simulations of the process, from the initial condition until the system reaches self-similar behaviour or until the point in time of interest from the experimental point of view, can be particularly hard to obtain with the aforementioned numerical approaches. Moreover, prediction of self-similar solutions can prove to be invaluable for extraction of system parameters that are otherwise hard to determine. Thus, it is important to be able to accurately predict self-similarity.

Motivated by these challenges, we addressed the problem from a different perspective. Taking into account the physics of the problem, we developed a variable transformation for both time and size that offers additional insight into the problem and allows for more efficient and general numerical simulation independently of the choices of: (a) final time, (b) breakage kernel and (c) breakage function. In section 2, we present the mathematical formulation of the problem and introduce the variable transformation. In section 3, we discuss the key features of a novel moving boundary numerical algorithm that was developed in order to solve the previously presented formulation. For the sake of clarity and continuity, the detailed

derivation of the algorithm is presented in the appendix. In section 4, we first show that our numerical results are in excellent agreement with a known analytical solution derived in [9]. We then use our algorithm to study the behaviour of the system as a function of model parameter values both asymptotically and transiently for the power-law family of breakage functions and for two families of breakage kernels: one symmetric and one asymmetric.

2. Mathematical formulation

Consider a population of particles which break continuously inside a volume V to give smaller particles. Let $N(x,t)\,\mathrm{d}x$ denote the number of particles per unit volume, which at time t have sizes between x and $x+\mathrm{d}x$. Then, for the case of binary breakage the problem has the following population balance formulation [8]:

$$\frac{\partial N(x,t)}{\partial t} = -a(x)N(x,t) + 2\int_x^{x_{\max}} a(y)\,p(x,y)N(y,t)\,\mathrm{d}y \tag{1}$$

subject to an initial condition:

$$N(x,0) = N_o(x), \tag{2}$$

where $x_{\max}$ is the maximum possible particle size at time t. Since any breakage process can only decrease the size of particles, $x_{\max}$ must always be smaller than its initial value. We will define $x_{\max}$ at each point in time by requiring that there exist no particles at this size:

$$N(x_{\max},t) = 0. \tag{3}$$

As can be seen from equation (1) the binary breakage process is fully characterized by the breakage function $a(x)$, which describes the rate by which a particle of size x breaks to give smaller particles and the breakage kernel or partition probability density function $p(x,y)$, which describes the probability that a mother particle with size y will produce upon breakage a daughter particle with size x and a daughter particle with size $y-x$. Since we assume that volume and mass are conserved at each breakage event, $p(x,y)$ needs to satisfy the constraint:

$$p(x,y) = p(y-x,y). \tag{4}$$

Moreover, since $p(x,y)$ is a probability density function, it should also satisfy the normalization constraint:

$$\int_0^y p(x,y)\,\mathrm{d}x = 1 \qquad p(x,y) = 0, \quad x \geqslant y. \tag{5}$$

Using properties (4) and (5), we can easily show that $p(x,y)$ satisfies the fact that the total volume of the two particles obtained from the break-up of a mother particle of volume y must be equal to y:

$$2\int_0^y x\,p(x,y)\,\mathrm{d}x = y. \tag{6}$$

In this work, we will consider the family of the most frequently used power-law breakage functions:

$$a(x) = x^L. \tag{7}$$

We will also consider breakage kernels of the form

$$p(x,y) = \frac{1}{y}\frac{\Gamma(2q+2)}{\Gamma(q+1)\Gamma(q+1)}\left(\frac{x}{y}\right)^q\left(1-\frac{x}{y}\right)^q \tag{8}$$

where Γ denotes the gamma distribution. Note that $p(x, y)$ is of the form: $p(x, y) = \frac{1}{y} v\left(\frac{x}{y}\right)$, where $v(z)$ is a symmetric beta distribution with a parameter of q. Thus, $p(x, y)$ is of the homogeneous type [20].

Taking the zeroth moment of equation (1) and using property (5) we obtain the dynamics of the particle density denoted by $m_o(t)$:

$$\frac{\mathrm{d}m_0}{\mathrm{d}t} = \int_0^{x_{\max}} a(x) N(x, t)\, \mathrm{d}x \tag{9}$$

which clearly shows that the particle density asymptotically approaches infinity.

Moreover, taking the first moment of equation (1) and applying property (6) we can easily see that the first moment of the distribution, which can be thought as a measure of the volume or mass density of the population is conserved during a breakage process (i.e. $\frac{\mathrm{d}m_1}{\mathrm{d}t} = 0$).

Now, let us derive the equation for the number density function $n(x, t)$ defined as

$$n(x, t) = \frac{N(x, t)}{m_o}. \tag{10}$$

Substituting equation (10) into equation (9) we obtain the dynamics of the zeroth moment as a function of the number density function:

$$\frac{\mathrm{d}m_o}{\mathrm{d}t} = m_o \int_0^{x_{\max}} a(x) n(x, t)\, \mathrm{d}x. \tag{11}$$

Substituting equation (10) into equation (1), dividing both sides of the equation with m_{o} and utilizing equation (11) yields

$$\frac{\partial n(x, t)}{\partial t} = -a(x) n(x, t) + 2 \int_x^{x_{\max}} a(y) p(x, y) n(y, t)\, \mathrm{d}y - n(x, t) \int_0^{x_{\max}} a(x) n(x, t)\, \mathrm{d}x. \tag{12}$$

As opposed to the original equation (1), equation (12) is nonlinear. Taking the first moment of equation (12) and utilizing the fact that the first moments of the first two terms in the right-hand side of equation (12) should vanish due to conservation of volume/mass during breakage, we derive the equation for the average size of the population $\langle x \rangle$:

$$\frac{\mathrm{d}\langle x \rangle}{\mathrm{d}t} = -\langle x \rangle \int_0^{x_{\max}} a(x) n(x, t)\, \mathrm{d}x \tag{13}$$

It is obvious from equation (13) that the average particle size decreases with time. Thus, $\langle x \rangle(t) \xrightarrow{\langle x \rangle(t) \to 0} 0$. We exploit this observation and define a dimensionless time as follows:

$$\tau = -\ln\left(\frac{\langle x \rangle}{\langle x_o \rangle}\right) \tag{14}$$

where $\langle x_o \rangle$ is the average size of the initial distribution. Note that $\tau \xrightarrow{\langle x \rangle(t) \to 0} \infty$. Therefore, the dimensionless time defined by equation (14) is a good measure of real time. We further define the dimensionless particle size as follows:

$$z = \frac{x}{\langle x \rangle}. \tag{15}$$

Finally, we define a new particle size number density function:

$$f(z, \tau)\, \mathrm{d}z = n(x, t)\, \mathrm{d}x. \tag{16}$$

Using the transformation (14)–(16) and the fact that the breakage kernel is homogeneous, equation (12) yields

$$\frac{\partial f}{\partial \tau} = -\frac{\partial (z f)}{\partial z} + \frac{-a(z) f(z, \tau) + 2 \int_z^{z_{\max}} a(w) p(z, w) f(z, \tau)\, \mathrm{d}w}{\int_0^{z_{\max}} a(z) f(z, \tau)\, \mathrm{d}z} - f(z, \tau). \tag{17}$$

Equation (17) is subject to an appropriate initial condition, related to the initial condition of the original problem as follows:

$$f(z,0) = \frac{\langle x_o \rangle N_o(x)}{m_{\mathrm{o,o}}} \equiv f_o(z) \tag{18}$$

where $m_{\mathrm{o,o}}$ is the initial particle density. Since $f(z,\tau)$ is a number density function, it should also satisfy the normalization constraint:

$$\int_0^{z_{\max}} f(z,\tau)\,\mathrm{d}z = 1. \tag{19}$$

The value of $z_{\max}$ is implicitly determined at each point in dimensionless time by the requirement:

$$f(z_{\max},\tau) = 0. \tag{20}$$

Taking the first moment of equation (17) and using equation (20) we find that the average of $f(z,\tau)$ must always be 1:

$$\int_0^{z_{\max}} z f(z,\tau)\,\mathrm{d}z = 1. \tag{21}$$

Thus, the problem under consideration in the transformed coordinate system consists of equations (17)–(21). In order to find the real time t, which corresponds to each value of the dimensionless time τ, one needs to solve the following non-autonomous differential equation which is obtained by employing equations (13)–(16):

$$\frac{\mathrm{d}t}{\mathrm{d}\tau} = \frac{\exp(L\tau)}{\langle x_o \rangle^L} \frac{1}{\int_0^{z_{\max}} a(z) f(z,\tau)\,\mathrm{d}z}. \tag{22}$$

Finally, the dynamics of the particle density are obtained from equation (11) with the use of equations (13) and (14):

$$\frac{\mathrm{d}m_o}{\mathrm{d}\tau} = m_o \Rightarrow m_o(\tau) = m_{\mathrm{o,o}}\,\exp(\tau). \tag{23}$$

By comparing equations (12) and (17) we observe that the aforementioned transformation added a convection term to the right-hand side of equation (17). Note also that the steady-state version of equation (17) obtained by setting the dimensionless time derivative equal to zero is identical to the equations presented by Cheng and Redner [16], describing the self-similar solution of the breakage equation. Thus, indeed this formulation can predict the full time evolution of the breakage process from the initial condition up to the point where the system reaches self-similar behaviour and beyond, if necessary, thus satisfying one of the objectives of this work. In addition, transforming the population balance equation in the new coordinate system offers explicit, exact knowledge of the mean particle size and particle density at each point in dimensionless time through equations (14) and (23), respectively. The corresponding actual time can be obtained through integration of equation (24), that can easily be transformed in an autonomous form through the transformation: $t(\tau) = \sigma(\tau)\frac{\exp(L\tau)}{\langle x_o \rangle^L}$.

3. Numerical solution

For the numerical solution of the problem we developed a tau-spectral method to approximate the solution in the dimensionless space coordinate, using Legendre basis functions. Since $z_{\max}$ is not *a priori* known and in order to increase computational efficiency, we posed the problem in a moving boundary formulation and used the mathematical model to derive the dynamics of the moving boundary. For the time integration of the resulting system of ordinary differential

equations (ODEs) we used the Runge–Kutta fourth-order time integrator. We also developed a zeroth-order continuation algorithm to find the steady-state solutions of equations (18)–(22) for the entire region of the model parameter space.

The number of degrees of freedom and time step necessary for accurate approximations is a function of the parameters of the problem and the initial condition. Since one of the main focuses of our work was to examine the effect of model parameter values and initial condition on both the transient and asymptotic behaviour of the system, we used various values for n and $\mathrm{d}\tau$ ($30 \leqslant n \leqslant 70$ and $10^{-6} \leqslant \mathrm{d}\tau \leqslant 10^{-3}$). A representative simulation with $n = 40$, $\mathrm{d}\tau = 10^{-4}$ and integration up to final dimensionless time of 5 (corresponding to a final mean size which is less than 0.007 of the initial mean) required less than 8 s in an Opteron 2.2 GHz. Although this estimate is typical, in some of the simulations that will be presented in the following, either less or more refined grid spacings were used.

For the sake of clarity of the presentation, the detailed derivation of the numerical algorithm is given in the appendix. The high computational efficiency of this algorithm is due to the combination of the following facts: (a) the transformation (14)–(16) not only allows the prediction of self-similarity but also avoids approximation of the solution when the mean particle size becomes very small, (b) the moving boundary formulation allows approximation of the solution only in the region where the solution is appreciably different from zero, (c) the convergence properties of Legendre polynomials are excellent for the problem under consideration and (d) the numerical stability limit of the time integrator employed is high for the solution of population balance equations.

4. Results and discussion

In the following, we will employ the algorithm to study the behaviour of the system for different breakage kernels and breakage rates. To validate our numerical algorithm we will first compare our simulation results with known analytical solutions. In the other cases where an analytical solution was not available, we performed exhaustive numerical simulations with refined grids in both space and time and calculated the $L2$ norms of the differences between the numerical solutions corresponding to different grids. In all cases, we achieved convergence. In fact, the order of convergence was exponential, which is a direct consequence of the use of spectral methods for the approximation of the size distribution [25].

4.1. Symmetric breakage kernels

In the special case of $L = 2$ and $q = 0$, Ziff and McGrady [9] derived an analytical expression of the breakage equation (1) for a general initial condition $N(x, 0)$:

$$N(x,t) = \mathrm{e}^{-tx^2}\left[N(x,0) + 2t\int_x^\infty yN(y,0)\,\mathrm{d}y\right]. \tag{24}$$

In order to verify the validity of our numerical algorithm, we compared our numerical results with the analytical solution (1) for a Gaussian initial condition with a mean of 5000 (arbitrary units) and a standard deviation of 10%. We used 35 degrees of freedom and a time step of 10^{-4} in this simulation. We integrated the equations up to dimensionless time of 5, corresponding to a final mean size which is less than 0.007 of the initial mean.

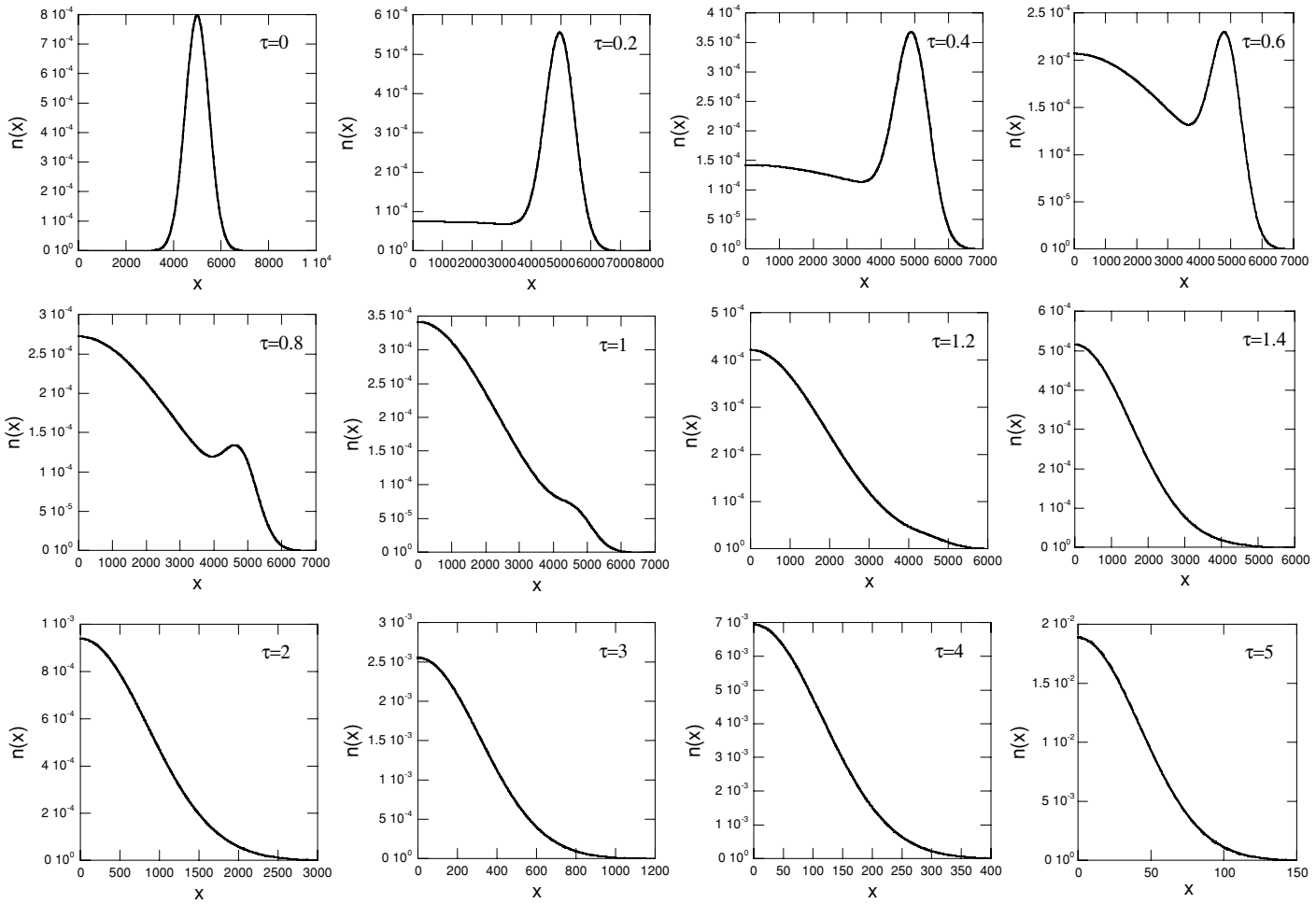

Figure 1. Comparison between numerical and analytical solutions from [9] for the case $L = 2$ and $q = 0$ for the number density function $n(x)$ at various points in dimensionless time.

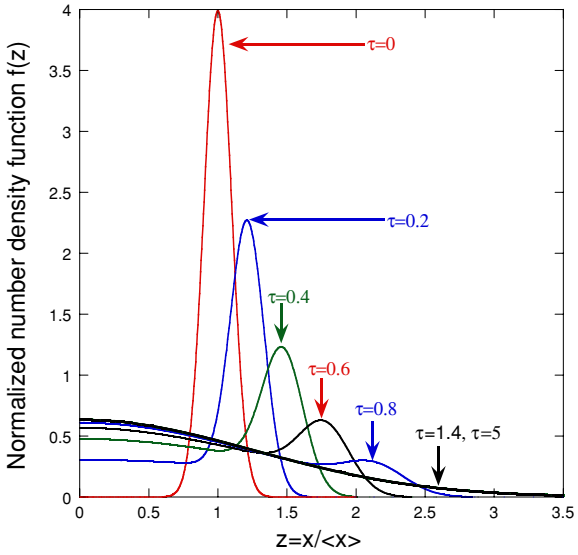

Figure 2. Comparison between numerical and analytical solutions from [9] for the case $L = 2$ and $q = 0$ for the normalized number density function $f(z)$ at various points in dimensionless time.

Figure 1 shows the comparison at different points in time for the number density function $n(x, t)$. First, note that the numerical and analytical predictions are virtually indistinguishable, thus proving the validity of the numerical algorithm. The maximum error that was observed in the simulation occurred at $x = 0$ and it remained less than 10^{-3} for the entire duration of the simulation run. Furthermore, by looking at the values in the x and y axes, one can observe that the number density function does not reach a steady state. As expected, $n(x, t)$ continuously moves towards lower sizes. The initial peak and a new one appears at lower sizes due to the continuous breakage of the bigger particles. However, after an initial lag of approximately 1.4 in dimensionless time, the number density function adopts a monotonically decreasing shape. The highest value is observed at $x = 0$, which is a direct consequence of the fact that the breakage kernel is independent of the size of the daughter fragment, since $q = 0$.

Figure 2 shows the corresponding predictions for the normalized number density function $f(z, \tau)$. Note that, contrary to $n(x, t)$, $f(z, \tau)$ reaches a time-invariant state right at the time when $n(x, t)$ adopts its monotonically decreasing shape around $\tau = 1.4$, which corresponds to a mean size that is approximately as high as 25% of the initial mean size. The prediction of such self-similar behaviour for $n(x, t)$ is in agreement with the theoretical results presented by many investigators (see [16] for example) and can be very useful in extracting system parameters for breakage processes, especially if it is attained that early in the evolution of the process.

We note that self-similar behaviour was observed for all values of q, and L and was verified through transient simulations. After establishing the validity of our numerical algorithm and making use of its generality, we proceeded to study the effect of the two-model parameter values on the shape of the asymptotic self-similar number density function. Figure 3 shows the effect of parameter q. Since the more concentrated the breakage kernel becomes around an equal split (higher value of q), the fewer the particles significantly smaller or bigger than the mean that will be created, the time-invariant number density function $f(z)$ becomes narrower. Note also (figure 4) that the sharper the breakage mechanism is (higher value of L),

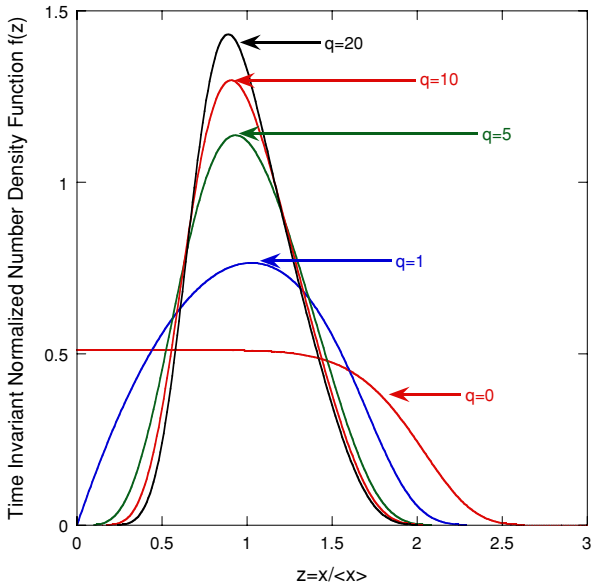

Figure 3. Effect of parameter q of the homogeneous symmetric breakage kernel on the self-similar solution for $L = 8$.

the narrower and the more symmetric the time-invariant number density function $f(z)$ becomes. The switch-like behaviour, characteristic of sharper breakage mechanisms leads to smaller differences in the breakage rates amongst particles that belong to the subpopulation existing below the breakage threshold, as well as amongst the particles that belong to the subpopulation above the breakage threshold. As a result, the time-invariant normalized number density function becomes narrower and more symmetric around the value of 1.

4.2. Asymmetric breakage kernels

Up to this point we have assumed that the breakage kernel was symmetric in the sense that the birth of two equally sized fragments is the most probable scenario in each breakage event. However, there are situations in which this might not be true. In this section, we will study the behaviour of the system when the mother particle partitions its material asymmetrically upon the two daughter fragments. There are many ways that one can define an asymmetric breakage kernel. For simplicity, let us assume that upon breakage one daughter fragment always receives a fraction r of the mother particle, while the other $1 - r$. If r is taken to always represent the smallest fraction of mother particle content that is inherited by one of the daughter particles we will have: $0 < r \leqslant 0.5$. Under this assumption the breakage kernel is formulated as follows:

$$p(x, y) = \frac{1}{2r}\delta(ry - x) + \frac{1}{2(1-r)}\delta((1-r)y - x) \tag{25}$$

where δ is the delta function. Clearly, the breakage kernel defined by equation (25) is discrete. For $r = 0.5$, we obtain the symmetric limit of this breakage kernel. It is easy to see that (25) satisfies the basic properties of $p(x, y)$ in a binary breakage process. Substituting this expression into equation (12), we obtain (instead of an integro-partial differential equation),

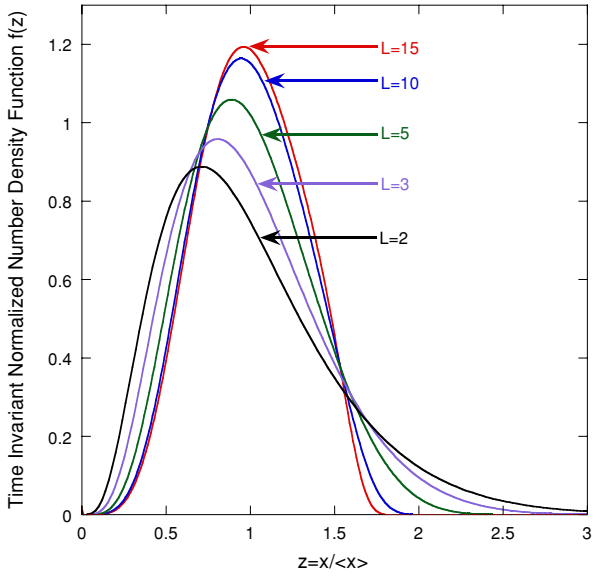

Figure 4. Effect of the sharpness of the breakage mechanism (parameter L) on the self-similar solution for $q = 5$ for the case of a symmetric breakage kernel.

a functional partial differential equation (FPDE) for the number density function dynamics:

$$\frac{\partial n(x,t)}{\partial t} = -a(x)n(x,t) + \frac{1}{r}a\left(\frac{x}{r}\right)n\left(\frac{x}{r},t\right) + \frac{1}{1-r}a\left(\frac{x}{1-r}\right)n\left(\frac{x}{1-r},t\right) - n(x,t)\int_0^{x_{\max}} a(x)n(x,t)\,\mathrm{d}x. \tag{26}$$

It is easy to show that applying the same transformation (14)–(16) to (26), leads to the following equation for the dynamics of the normalized number density function:

$$\frac{\partial f}{\partial \tau} = -\frac{\partial (zf)}{\partial z} + \frac{-a(z)f(z,\tau) + \frac{1}{r}a\left(\frac{x}{r}\right)f\left(\frac{z}{r},\tau\right) + \frac{1}{1-r}a\left(\frac{z}{1-r}\right)f\left(\frac{z}{1-r},\tau\right)}{\int_0^{z_{\max}} a(z)f(z,\tau)\,\mathrm{d}z} - f(z,\tau) \tag{27}$$

subject to the same normalization conditions (19) and (21). Minor modifications in our steady state and transient codes allowed us to successfully simulate the breakage process in the case of asymmetric breakage kernels.

Similar to the symmetric breakage kernel case, the number density function $n(x,t)$ does not reach a time-invariant behaviour, while the transformed, normalized number density function $f(z,\tau)$ does. Thus, self-similarity is also a feature of asymmetric breakage as was also shown by Kostoglou [20] using theoretical tools. Figure 5 shows the effect of the partitioning ratio r on the time-invariant shape of $f(z,\tau)$. Note that higher asymmetry in the breakage kernel (lower value of r) leads to broader number density functions. More importantly, note that as opposed to the case of symmetric breakage kernel, the time-invariant, normalized number density function becomes bimodal for breakage kernels that are asymmetric beyond a certain threshold. The value of the threshold in r, below which the bimodality pattern appears, is a monotonically increasing function of the sharpness of the breakage mechanism (parameter L). This important qualitative difference with the symmetric breakage kernel case is in qualitative agreement with the recent theoretical results of Kostoglou [20] and can be understood as follows.

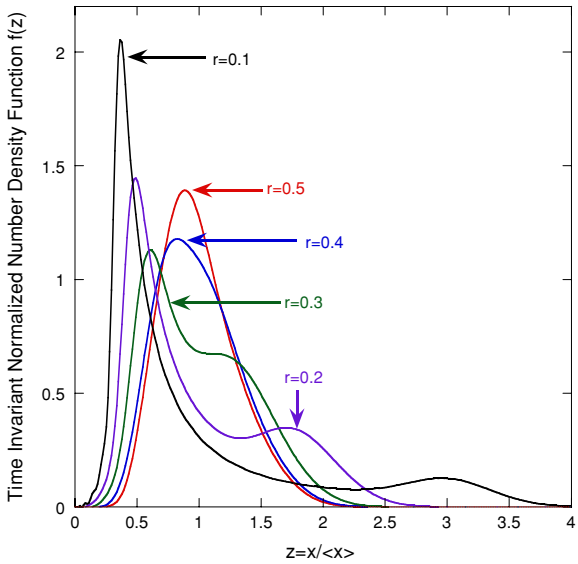

Figure 5. Effect of the extent of asymmetry r of the asymmetric breakage kernel on the self-similar solution for $L = 5$.

The appearance of multimodal number density functions transiently (see also figure 7) as well as asymptotically is a result of the complex interplay between the breakage and partitioning mechanisms as well as convection in the dimensionless size domain (z domain). In particular, the initial, transient development of multiple subpopulations is a consequence of the fact that bigger particles break faster than smaller particles and that our initial condition is rather narrow. The number of distinct subpopulations (modes) that will be created transiently is a function of the initial particle distribution, the sharpness of the breakage mechanism and the extent of asymmetry in breakage. Broad initial distributions facilitate the appearance of more distinct subpopulations of particles as has been seen in many transient simulations of the system. Moreover, the sharper the breakage mechanism is (higher value of L) or the more asymmetric the breakage is (low values of r), the smaller the number of distinct subpopulations that will be created.

The dynamics of the normalized number density function are influenced by convection in the normalized particle size domain (see the first term in the right-hand side of equation (27)). All particles move towards bigger dimensionless sizes, with a rate that is equal to their size. Therefore, convection contributes towards solidifying the initial separation of the population into subpopulations, since the bigger particles move faster towards higher dimensionless sizes than their smaller peers. On the other hand, breakage of bigger particles is faster than that of the smaller particles and, contrary to convection, tends to 'return' particles to lower dimensionless sizes. Therefore, breakage tends to bring the different subpopulations together for large dimensionless times thus, promoting unimodal shapes of the number density function. The final outcome strongly depends on the extent of asymmetry in the breakage kernel. If partitioning is nearly symmetric, the size separation between the subpopulations is small. Hence, there is enough time for the breakage process to asymptotically bring the subpopulations together in a unimodal number density function. If, on the other hand, partitioning is more asymmetric than a certain threshold, there is not enough time for the subpopulation at lower sizes to 'catch-up' with the subpopulation at higher sizes, thus leading to bimodal number density functions asymptotically. The fact that at most two modes appear

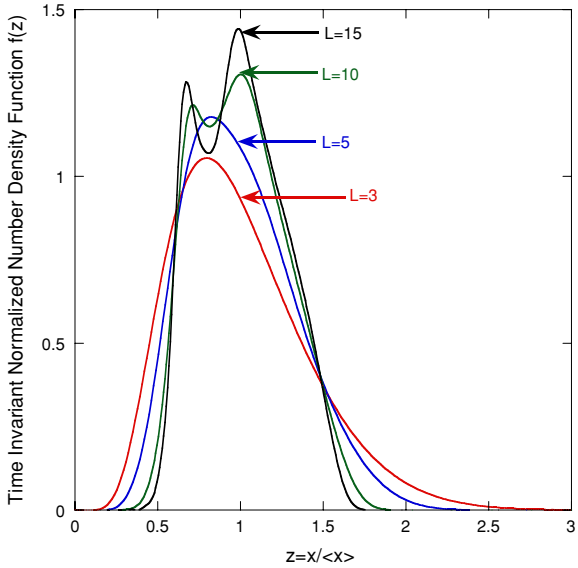

Figure 6. Effect of the sharpness of the breakage mechanism (parameter L) on the self-similar solution for $r = 0.4$ and for the case of asymmetric breakage kernels.

asymptotically (although more may appear transiently) is a direct consequence of binary breakage. We expect that multimodal steady-state number density functions will exist if each breakage event leads to the production of more than two particles.

We have already seen in figure 5 that high asymmetry in the breakage kernel leads asymptotically to broader and bimodal number density functions. One might be tempted to think that asymptotic bimodality is always accompanied by an increase in the standard deviation of the normalized, time-invariant number density function. However, this is not the case as can be seen in figure 6, which shows the effect of L on the shape of $f(z)$ asymptotically. Note that sharper breakage (higher values of L) leads to bimodal but narrower number density functions for a given extent of asymmetry in the breakage kernel. The decrease in the standard deviation for larger values of L has the same qualitative explanation as for the case of the symmetric breakage kernel. The appearance of bimodal number density functions for sharper breakage mechanisms is a result of the clearer size separation between distinct subpopulations initially, which cannot be compensated even for nearly symmetric breakage kernels ($r = 0.4$). This in turn leads to the observed bimodality for values of L higher than a threshold.

The results presented in figures 5 and 6 were also verified through extensive transient simulations. Starting from a variety of initial conditions, the system reaches the number density functions presented in figures 5 and 6, thus verifying their stability. Figure 7 shows a representative transient simulation for the case of $r = 0.3$. Note that initially, multimodal number density functions appear, which are in qualitative agreement with the work of Kostoglou and Karabelas [14] who employed the analytical method of successive generations to also show multimodality at early times in the case of the homogeneous erosion kernel. However, note that after approximately $\tau = 7$ the system starts to approach the final bimodal number density function shown in figure 5. Self-similarity is attained at approximately $\tau = 11$. The dimensionless time required to reach self-similarity decreases as breakage becomes more asymmetric (lower values of r). Note that despite the early erratic dynamical behaviour of the system due to the development of multimodal number density functions as a result of the

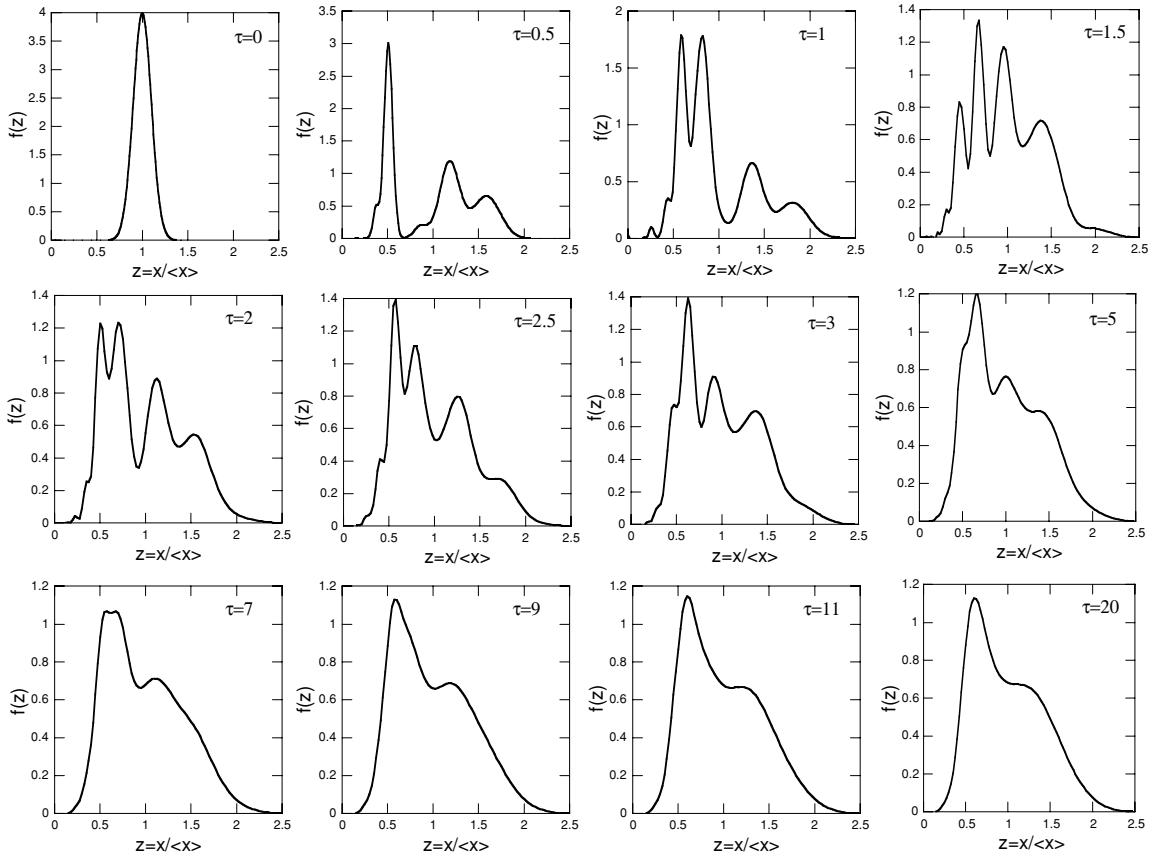

Figure 7. Dimensionless time evolution of the normalized number density function $f(z, \tau)$ for $L = 5$ and for the asymmetric breakage kernel with $r = 0.3$.

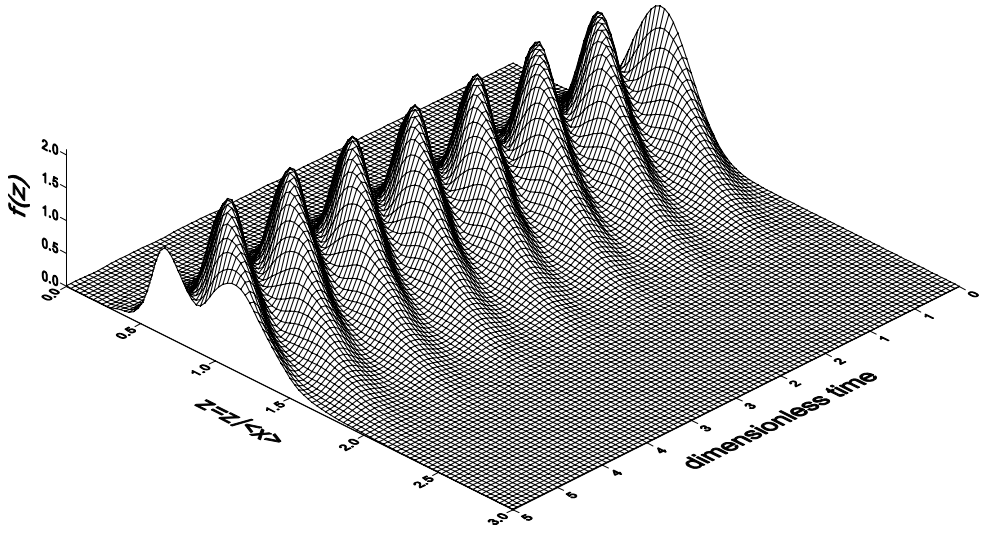

Figure 8. Dimensionless time evolution of the normalized number density function $f(z, \tau)$ for $L = 5$ and for the symmetric limit of the asymmetric breakage kernel ($r = 0.5$).

discrete nature of the breakage kernel, the numerical algorithm manages to successfully simulate the process from the initial condition up to the point in time where it reaches self-similar behaviour.

There is one notable exception where the system does not exhibit self-similar behaviour in the traditional sense. This is the case of the symmetric limit of the breakage kernel (25) ($r = 0.5$), which deserves special consideration due to its unique dynamical characteristics. Figure 8 shows a representative transient simulation for $L = 5$. Note that the system does not reach the time-invariant state presented in figure 5. Instead, it exhibits sustained oscillations.

This qualitative behaviour was found to be independent of the sharpness of the breakage mechanism as well as the initial condition, as shown in figures 9 and 10. In all cases where $r = 0.5$, the system oscillates around the unstable time-invariant number density function corresponding to the specific value of L. The sharpness of the division mechanism influences the amplitude of the oscillations as shown in figure 9. Sharper breakage leads to higher oscillation amplitude, while the oscillation centre becomes lower, since sharper breakage decreases the standard deviation of the corresponding unstable, time-invariant number density function. Moreover, narrower initial conditions lead to more pronounced oscillations around the same centre, as figure 10 shows. Finally, note that in all cases, the period of the oscillation remains exactly the same, and, as found through computations equal to: $T = \ln 2$.

To understand the existence of the oscillations in the special case of perfectly equal partitioning, consider two particles which initially have the same size normalized around the mean (same z value). Due to the linearity of the convection term in equation (27), they will both 'grow' in the z-domain with the same rate. They will break simultaneously with the same size and each mother particle will produce two identical daughter particles. All four of the newborn particles will have the exact same z value, and they will re-start 'growing' in the z-domain with the same rate since they have equal dimensionless sizes, until they break again with the same size giving birth to eight new particles with equal dimensionless sizes. This phenomenon will keep repeating itself for all particles in the population, thus giving rise to the

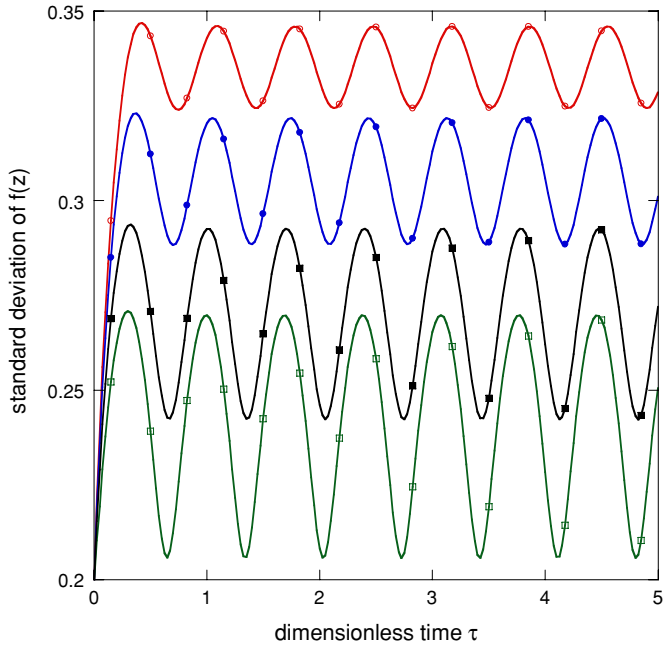

Figure 9. The effect of the sharpness of the breakage mechanism (parameter L) on the oscillation dynamics of the standard deviation of $f(z, \tau)$ for the symmetric limit of the asymmetric breakage kernel ($r = 0.5$). Open circles: $L = 4$; filled circles: $L = 5$; filled squares: $L = 7$; open squares: $L = 10$.

observed sustained oscillations. This is not the case if partitioning is asymmetric ($r < 0.5$) or even if partitioning is symmetric but not discrete, such as in equation (8). Although the highest probability at each breakage event is to produce two equally sized particles when partitioning is symmetric and not discrete, there is still the probability of producing two daughter particles of different sizes. As a result, the two newborn particles 'grow' in the z-domain with different rates, break at different times, and therefore, the perfect periodic behaviour is destroyed.

Diekmann and co-workers have worked with the cell population balance model with equal partitioning [26], which is remarkably similar to equation (27) for $r = 0.5$. The basic difference originates from the fact that the total dimensionless breakage rate $\int_0^{z_{\max}} a(z) f(z, \tau)\, \mathrm{d}z$ becomes dependent on dimensionless time for $r = 0.5$. Due to the fact that in equation (27) both terms are normalized with the total breakage rate, the breakage and birth rates also become dependent on dimensionless time in our formulation. In contrast, in the case of the FPDE they studied, the division and birth rates were time independent. Using semi-group theory, Diekmann and co-workers have shown that when the single-cell growth rate is linear with a proportionality constant of 1, the number density function will oscillate with a period of $\ln 2$. Although in our case there is no growth in the real size domain, there is artificial growth or convection in the dimensionless size domain, which is linear with a proportionality constant of 1. Thus, our prediction for the existence of a periodic solution as well as for the actual value of the period of the oscillation is consistent with the theoretical analysis of Diekmann and co-workers [26]. It will be interesting to develop possible extensions of their theoretical work in the case of the FPDE (27).

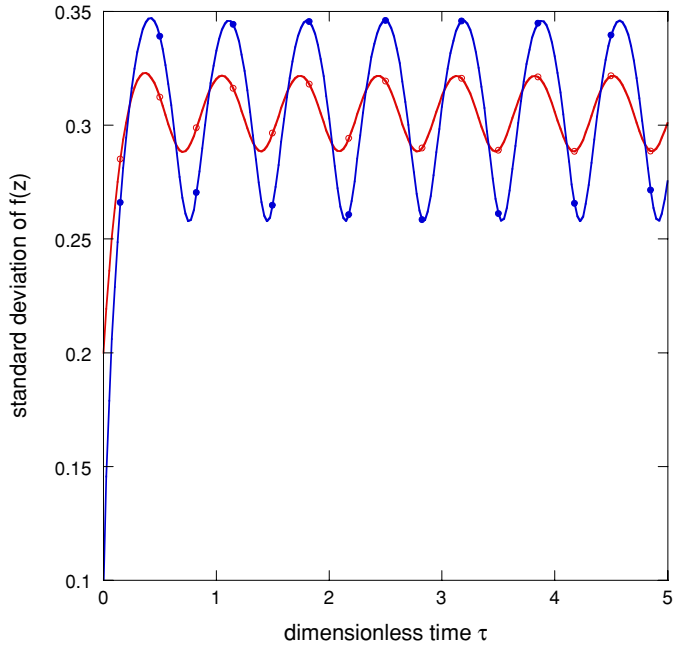

Figure 10. The effect of the initial standard deviation on the oscillation dynamics of the standard deviation of $f(z,\tau)$ for the symmetric limit of the asymmetric breakage kernel ($r = 0.5$). Open circles: broad initial distribution ($\sigma(0) = 0.2$); filled circles: narrow initial distribution ($\sigma(0) = 0.1$).

5. Summary and conclusions

In this work we studied the general binary breakage problem for the power-law family of breakage functions and two families of breakage kernels: one symmetric and one asymmetric. We transformed the original problem into a new coordinate system which clearly highlighted the self-similar behaviour of the process independently of the parameters of the problem. Moreover, we developed a novel, moving boundary numerical algorithm which can simulate the process rapidly and accurately. The algorithm consists of first recasting the problem in a moving boundary formulation and then utilizing orthonormal Legendre basis functions for the approximation of the solution in the dimensionless size domain, in conjunction with time explicit Runge–Kutta fourth-order for the time integration. The numerical results were found to be in excellent agreement with known analytical results, thus verifying the validity of the code.

The developed numerical algorithm has several unique features, which render it very powerful when compared to other numerical algorithms that were presented in the literature in order to solve the general binary breakage problem. First, the transformation employed allows solving the modified problem in the coordinates which lead to a time-invariant state. This in turn prevents errors at large times that are associated with direct discretization of the original form of the problem. At the same time, the presented approach predicts the time-invariant distributions, which possess a variety of information that can be utilized to extract model parameter values. Moreover, the transformation allows analytical knowledge of the particle density at each point in time. In addition, the use of a moving boundary formulation in the transformed coordinate system offers more accuracy. This is because the degrees of freedom

employed in the simulation are used to approximate the distribution at each point in time only in the region of the domain where particles exist.

The presented numerical simulations have shown that the number density function with respect to particle size does not reach a genuine steady state as the mean particle size continuously decreases with time. However, the normalized around the mean number density function quickly reaches a time-invariant state, which can be used to extract key system parameters through comparison with experimental data. In the case of the family of symmetric beta distributions describing the partitioning of the mother particle into two daughter particles, it was found that sharper breakage functions lead to narrower and more symmetric time-invariant number density functions, while higher probability for exactly equal partitioning leads to narrower time-invariant number density functions.

We modelled the case of asymmetric breakage by assuming that each breakage event leads to the birth of one particle with a fraction r and another particle with a fraction $1 - r$ of the size of the mother particle. Contrary to the case of symmetric breakage kernels, where all asymptotic, normalized number density functions were unimodal, a high degree of asymmetry in the breakage kernel was found to asymptotically lead to bimodal and broader normalized number density functions. Furthermore, bimodality may also appear as a consequence of sharp breakage mechanisms even for moderately asymmetric breakage kernels. However, bimodality thus induced is accompanied by a decrease in the standard deviation of the asymptotic, normalized number density function.

The only case where a time-invariant, normalized number density function was not reached is the symmetric limit of the asymmetric breakage kernel. In this case, the normalized number density function exhibits sustained oscillations with a standard deviation that fluctuates around the value of the corresponding unstable solution of the steady-state problem. Sharper breakage mechanisms and narrower initial conditions lead to higher amplitude oscillations, while the period of the oscillation is always independent of the parameters of the problem and was found to be equal to $\ln 2$ in all cases. To the author's knowledge, this is the first time that sustained oscillations are predicted asymptotically in the context of pure breakage processes.

Due to the generality of the approach and numerical solution, the presented framework can prove to be a valuable tool in extracting system parameters from experimentally obtained time-invariant, normalized number density functions. Moreover, due to the low number of modes necessary to simulate the process, our numerical algorithm can be used as a basis for controller synthesis in breakage processes. This can prove to be a powerful approach especially if combined with approximate inertial manifold techniques used for model reduction in a variety of systems described by partial differential equations (see, e.g., [27]). Finally, the presented framework can easily be extended to multi-breakage processes with minor modifications.

Acknowledgment

Financial support by NIH/NIGMS through grant R01 GM071888 is gratefully acknowledged. The author would also like to thank the reviewers for many useful comments.

Appendix

In order to achieve higher computational efficiency, we treated the right boundary $z_{\max}$ as time dependent. Thus, we posed the problem in a moving boundary formulation. The moving

domain $[0, z_{\max}(\tau)]$ was mapped into the fixed computational domain $[0, 1]$ through the linear transformation:

$$z = z_{\max}(\tau)\xi, \qquad 0 \leqslant \xi \leqslant 1. \tag{A.1}$$

We also set

$$f(z, \tau)\,\mathrm{d}z = u(\xi, \tau)\,\mathrm{d}\xi. \tag{A.2}$$

Thus

$$f(z, \tau) = \frac{u(\xi, \tau)}{z_{\max}}. \tag{A.3}$$

Using equations (A.1)–(A.3) and the homogeneity of the breakage kernel, equation (17) becomes

$$\frac{\partial u}{\partial \tau} = \left(\frac{1}{z_{\max}}\frac{\mathrm{d}z_{\max}}{\mathrm{d}\tau} - 1\right)\frac{\partial(\xi u)}{\partial \xi} + \frac{-a(\xi)u(\xi, \tau) + 2\int_{\xi}^{1} a(\eta)p(\xi, \eta)u(\eta, \tau)\,\mathrm{d}\eta}{\int_0^1 a(\xi)u(\xi, \tau)\,\mathrm{d}\xi} - u(\xi, \tau) \tag{A.4}$$

subject to the initial condition:

$$u(\xi, 0) = \frac{\langle x_o\rangle N_o(x) z_{\max}(0)}{m_{\mathrm{o,o}}} \equiv u_{\mathrm{o}}(\xi). \tag{A.5}$$

To find the dynamics of the moving right boundary $z_{\max}$, which appear in equation (A.4), we take the time derivative of equation (20) and apply the chain rule:

$$\frac{\partial f(z_{\max}, \tau)}{\partial z}\frac{\mathrm{d}z_{\max}}{\mathrm{d}\tau} + \frac{\partial f(z_{\max}, \tau)}{\partial \tau} = 0. \tag{A.6}$$

Using the transformation (A.1)–(A.3), we obtain

$$\frac{\partial u(1, \tau)}{\partial \tau} = \frac{1}{z_{\max}}\frac{\mathrm{d}z_{\max}}{\mathrm{d}\tau}u(1, \tau). \tag{A.7}$$

Applying equation (A.4) to $\xi = 1$ and substituting into equation (A.7) yields the equation that determines the dynamics of $z_{\max}$:

$$\frac{1}{z_{\max}}\frac{\mathrm{d}z_{\max}}{\mathrm{d}\tau} = 1 + \frac{u(1, \tau) + 2u(1, \tau)\int_0^1 a(\xi)u(\xi, \tau)\,\mathrm{d}\xi}{\frac{\partial u(1,\tau)}{\partial \xi}\int_0^1 a(\xi)u(\xi, \tau)\,\mathrm{d}\xi}. \tag{A.8}$$

Moreover, the solution of equation (A.4) obeys the normalization constraint:

$$\int_0^1 u(\xi, \tau)\,\mathrm{d}\xi = 1. \tag{A.9}$$

Taking the time derivative of equation (A.9) we obtain

$$\int_0^1 \frac{\partial u}{\partial \tau}\,\mathrm{d}\xi = 0. \tag{A.10}$$

Furthermore, from equations (21) and (A.1) we obtain

$$z_{\max}\int_0^1 \xi u(\xi, \tau)\,\mathrm{d}\xi = 1 \quad \Rightarrow \quad z_{\max} = \frac{1}{\langle\xi\rangle} \tag{A.11}$$

where $\langle\xi\rangle$ is the mean value of $u(\xi, \tau)$. Taking the time derivative of equation (A.11) yields

$$\int_0^1 \xi\frac{\partial u}{\partial \tau}\,\mathrm{d}\xi = -\frac{1}{z_{\max}}\frac{\mathrm{d}z_{\max}}{\mathrm{d}\tau}\int_0^1 \xi u\,\mathrm{d}\xi. \tag{A.12}$$

Thus, the problem to be solved consists of equation (A.4) with the dynamics of $z_{\max}$ given by equation (A.8), subject to the initial condition (A.5) and the constraints (A.7), (A.10) and (A12).

We expand the solution in an infinite series of basis functions and retain only a finite number (n) of terms in the expansion:

$$u(\xi, \tau) = \sum_{j=1}^{n} c_j(\tau)\phi_j(\xi). \tag{A.13}$$

We chose Legendre basis functions due to their excellent convergence properties in approximating the solutions to a variety of problems in fixed domains with general boundary conditions [25]. In [0, 1] the Legendre basis functions are defined as follows:

$$\phi_i(\xi) = \sqrt{2i-1}\, P_i(\xi) \qquad i = 1, 2, \ldots \tag{A.14}$$

where the polynomials $P_i(x)$ are evaluated by the recursive formula:

$$\begin{aligned} &P_1(\xi) = 1 \qquad P_2(\xi) = 2\xi - 1 \\ &P_i(\xi) = \frac{2i-3}{i-1}(2\xi - 1)\, P_{i-1}(\xi) - \frac{i-2}{i-1}\, P_{i-2}(\xi) \qquad i = 3, 4, \ldots . \end{aligned} \tag{A.15}$$

The functions defined by equations (A.14) and (A.15) form an orthonormal set:

$$\int_0^1 \phi_i(\xi)\phi_j(\xi)\, \mathrm{d}\xi = \delta_{ij}. \tag{A.16}$$

To derive the dynamics of the time-dependent expansion coefficients, we apply the standard weighted residual approach. In particular we (a) substitute equation (A.13) into equation (A.4), (b) multiply by $\phi_i(\xi)$ both sides of the equation, (c) integrate over the entire domain [0, 1], and (d) apply the orthonormality condition (A.16) to obtain the following system of ordinary differential equations:

$$\frac{\mathrm{d}c_i}{\mathrm{d}\tau} = -\left(\frac{1}{z_{\max}}\frac{\mathrm{d}z_{\max}}{\mathrm{d}\tau} - 1\right)\sum_{j=1}^{n} G_{ij}c_j + \frac{1}{A_{\mathrm{o}}}\sum_{j=1}^{n}(-D_{ij} + B_{ij})c_j - c_i \tag{A.17}$$

where

$$G_{ij} = \int_0^1 \frac{\mathrm{d}\phi_i(\xi)}{\mathrm{d}\xi}\xi\, \phi_j(\xi)\, \mathrm{d}\xi \tag{A.18}$$

$$D_{ij} = \int_0^1 \phi_i(\xi)\, a(\xi)\, \phi_j(\xi)\, \mathrm{d}\xi \tag{A.19}$$

$$B_{ij} = \int_0^1 \phi_i(\xi)\left[\int_\xi^1 a(\eta)\, p(\xi, \eta)\, \phi_j(\eta)\, \mathrm{d}\eta\right]\mathrm{d}\xi \tag{A.20}$$

$$A_o = \sum_{j=1}^{n} c_j \int_0^1 a(\xi)\phi_j(\xi)\, \mathrm{d}\xi. \tag{A.21}$$

Substituting equation (A.13) into equation (A.8) yields

$$\frac{1}{z_{\max}}\frac{\mathrm{d}z_{\max}}{\mathrm{d}\tau} = 1 + \frac{(1 + 2A_o)\sum_{j=1}^{n} c_j(\tau)\phi_j(1)}{A_o \sum_{j=1}^{n} c_j(\tau)\frac{\mathrm{d}\phi_j(1)}{\mathrm{d}\xi}}. \tag{A.22}$$

Moreover, applying equation (A.13) into constraints (A.10) and (A.12) yields the constraints that the time derivatives of the expansion coefficients need to satisfy

$$\sum_{i=1}^{n} \frac{\mathrm{d}c_i}{\mathrm{d}\tau} \int_0^1 \phi_i(\xi)\,\mathrm{d}\xi = 0 \tag{A.23}$$

and

$$\sum_{i=1}^{n} \frac{\mathrm{d}c_i}{\mathrm{d}\tau} \int_0^1 \xi\phi_i(\xi)\,\mathrm{d}\xi = -\frac{1}{z_{\max}} \frac{\mathrm{d}z_{\max}}{\mathrm{d}\tau} \sum_{i=1}^{n} c_i \int_0^1 \xi\phi_i(\xi)\,\mathrm{d}\xi. \tag{A.24}$$

In order to ensure that the solution is consistent with equation (A.22), we need to impose equation (A.7) that was used to derive equation (A.8). Substituting equation (A.13) into equation (A.7) yields an additional constraint on the time derivatives of the expansion coefficients:

$$\sum_{i=1}^{n} \frac{\mathrm{d}c_i}{\mathrm{d}\tau} \phi_i(1) = \frac{1}{z_{\max}} \frac{\mathrm{d}z_{\max}}{\mathrm{d}\tau} \sum_{i=1}^{n} c_i\,\phi_i(1). \tag{A.25}$$

Thus, we transformed the problem into the system of ODEs (A.17), with the dynamics of $z_{\max}$ given by equation (A.22). These ODEs need to satisfy the constraints expressed by equations (A.23)–(A.25). For the time integration of this system, we applied the Runge–Kutta fourth-order method, which is known to be very appropriate for the numerical solution of population balance models due to the excellent compromise between accuracy, CPU time requirements and numerical stability that it offers [28–30].

References

[1] Ziff R M and McGrady E D 1986 Kinetics of polymer degradation *Macromolecules* **19** 2513–9

[2] Huang J, Guo X, Edwards B F and Levine A D 1996 Cut-off model and exact general solutions for fragmentation with mass loss *J. Phys. A: Math. Gen.* **29** 7639–58

[3] Kelley E G and Spottiswood D J 1982 *Introduction to Mineral Processing* (New York: Wiley)

[4] Mazzarotta B 1992 Abrasion and breakage phenomena in agitated crystal suspensions *Chem. Eng. Sci.* **47** 3105–11

[5] Hesketh R P, Etchells A W and Russell T W F 1991 Bubble breakage in pipeline flow *Chem. Eng. Sci.* **46** 1–9

[6] Fredrickson A G, Ramkrishna D and Tsuchyia H M 1967 Statistics and dynamics of Prokaryotic cell populations *Math. Biosci.* **1** 327–74

[7] Redner S 1990 *Statistical Models for the Fracture of Disordered Media* ed h J Hermann and S Roux (Amsterdam: Elsevier) chapter 10

[8] Ramkrishna D 2000 *Population Balances: Theory and Applications to Particulate Systems in Engineering* (San Diego, CA: Academic)

[9] Ziff R M and McGrady E D 1985 The kinetics of cluster fragmentation and depolymerization *J. Phys. A: Math. Gen.* **18** 3027–37

[10] McGrady E D and Ziff R M 1987 'Shattering' transition in fragmentation *Phys. Rev. Lett.* **58** 892–5

[11] Ziff R M 1991 New solutions to the fragmentation equation *J. Phys. A: Math. Gen.* **24** 2821–8

[12] Kostoglou M, Dovas S and Karabelas A J 1997 On the steady state size distribution of dispersions in breakage processes *Chem. Eng. Sci.* **52** 1285–99

[13] Kostoglou M and Karabelas A J 1998 Theoretical analysis of the steady state particle size distribution in limited breakage processes *J. Phys. A: Math. Gen.* **31** 8905–21

[14] Kostoglou M and Karabelas A J 2001 On the breakage problem with a homogeneous erosion type kernel *J. Phys. A: Math. Gen.* **34** 1725–40

[15] Filippov A F 1961 On the distribution of the sizes of particles which undergo splitting *Theory Prob. Appl.* **4** 275–94

[16] Cheng Z and Redner S 1988 Scaling theory of fragmentation *Phys. Rev. Lett.* **60** 2450–3

[17] Friedlander S K and Wang C S 1966 The self-preserving particle size distribution for coagulation by Brownian motion *J. Colloid Interface Sci.* **22** 126–32

[18] Treat R P 1997 On the similarity solution of the fragmentation equation *J. Phys. A: Math. Gen.* **30** 2519–43
[19] Madras G and McCoy B J 1998 Time evolution to similarity solutions for polymer degradation *AIChE J.* **44** 647–55
[20] Kostoglou M 2003 Exact self-similar solutions to the fragmentation equation with homogeneous discrete kernel *Physica* A **320** 84–96
[21] Hill P J and Ng K M 1995 New discretization procedure for the breakage equation *AIChE J.* **41** 1204–16
[22] Hill P J and Ng K M 1996 Statistics of multiple particle breakage *AIChE J.* **42** 1600–11
[23] Vanni M 1999 Discretization procedure for the breakage equation *AIChE J.* **45** 916–9
[24] Liu Y and Tade M O 2004 New wavelet-based adaptive method for the breakage equation *Powder Technol.* **139** 61–8
[25] Diekmann O, Heijmans H J A M and Thieme H R 1984 On the stability of the cell size distribution *J. Math. Biol.* **19** 227–48
[26] Gottlieb D and Orszag S A 1977 *Numerical Analysis of Spectral Methods: Theory and Applications* (Philadelphia, PA: SIAM)
[27] Christofides P D 2001 *Nonlinear and Robust Control of Partial Differential Equation Systems: Methods and Applications to Transport-Reaction Processes* (Boston, MA: Birkhauser)
[28] Mantzaris N V, Daoutidis P and Srienc F 2001a Numerical solution of multivariable cell population balance models: I. Finite difference methods *Comput. Chem. Eng.* **25** 1411–40
[29] Mantzaris N V, Daoutidis P and Srienc F 2001b Numerical solution of multivariable cell population balance models: II. Spectral methods *Comput. Chem. Eng.* **25** 1441–62
[30] Mantzaris N V, Daoutidis P and Srienc F 2001c Numerical solution of multivariable cell population balance models: III. Finite element methods *Comput. Chem. Eng.* **25** 1463–81